

Effects of Coulomb interactions on spin states in vertical semiconductor quantum dots

S. Tarucha^{1,2,*}, D.G. Austing², S. Sasaki², Y. Tokura², W. van der Wiel³, L.P. Kouwenhoven³

¹Department of Physics and ERATO Mesoscopic Correlation Project, University of Tokyo, 7-3-1, Hongo, Bunkyo-ku, Tokyo, 113-0033, Japan

²NTT Basic Research Laboratories, 3-1, Morinosato Wakamiya, Atsugi-shi, Kanagawa 243-0198, Japan

³Department of Applied Physics and ERATO Mesoscopic Correlation Project, Delft University of Technology, P.O. Box 5046, 2600 GA Delft, The Netherlands

Received: 14 April 2000/Accepted: 17 April 2000/Published online: 6 September 2000 – © Springer-Verlag 2000

Abstract. The effects of direct Coulomb and exchange interactions on spin states are studied for quantum dots contained in circular and rectangular mesas. For a circular mesa a spin-triplet favored by these interactions is observed at zero and nonzero magnetic fields. We tune and measure the relative strengths of these interactions as a function of the number of confined electrons. We find that electrons tend to have parallel spins when they occupy nearly degenerate single-particle states. We use a magnetic field to adjust the single-particle state degeneracy, and find that the spin-configurations in an arbitrary magnetic field are well explained in terms of two-electron singlet and triplet states. For a rectangular mesa we observe no signatures of the spin-triplet at zero magnetic field. Due to the anisotropy in the lateral confinement single-particle state degeneracy present in the circular mesa is lifted, and Coulomb interactions become weak. We evaluate the degree of the anisotropy by measuring the magnetic field dependence of the energy spectrum for the ground and excited states, and find that at zero magnetic field the spin-singlet is more significantly favored by the lifting of level degeneracy than by the reduction in the Coulomb interaction. We also find that the spin-triplet is recovered by adjusting the level degeneracy with magnetic field.

PACS: 72.20.My; 73.23.Hk; 73.61.Ey

Transport measurements of semiconductor nanostructures have revealed a variety of phenomena associated with the quantization for both energy level and charge. Resonant tunneling through a small quantum box, which is weakly coupled to the leads, shows a series of current peaks when the Fermi energy in the emitter lead and discrete zero-dimensional (0D) levels in the box are energetically aligned [1]. This is well understood within the framework of single-particle tunneling theory, which does not incorporate the effect of Coulomb interactions. On the other hand, when electrons are effectively trapped in the box during transport, the box acts as a Coulomb

island, and the effect of Coulomb interactions leads to the quantization of charge [2]. The trapping of an extra electron raises the electrostatic potential of the island by the charging energy. This energy regulates one by one the number of electrons on the island, and gives rise to oscillations in the tunneling conductance (Coulomb-blockade oscillations) when the gate voltage is swept. These oscillations are usually periodic and explained using an orthodox Coulomb-blockade theory when the number of electrons or the island size is “large” [2]. However, in a “small” dot holding just a few electrons, both effects of energy and charge quantization significantly influence the electronic states (“many-particle states”). Such a system can be regarded as an artificial atom [3]. Recently we have fabricated vertical quantum dots in circular mesas [4]. Associated with the rotational symmetry, as well as the parabolicity in the in-plane two-dimensional (2D) harmonic confinement potential, atom-like properties such as shell-filling and obeyance of Hund’s first rule are all observed [5]. The high cylindrical symmetry of the circular dot leads to maximal level degeneracy of single-particle states for the 2D parabolic confinement. Consecutive filling of each set of degenerate 0D states is directly responsible for the characteristic shell structure. On the other hand, Hund’s first rule is associated with the interaction effects for the electron filling amongst nearly degenerate states. Ferromagnetic filling is then favored amongst half-filled degenerate states in each shell. Breaking the circular symmetry by deforming the lateral confining potential, lifts the degeneracies present in a circular dot, and destroys the distinctive shell structure for the circle, and modifies other atomic-like properties [6, 7].

In this paper we study the effects of Coulomb interactions on the spin states in the circular and elliptically deformed quantum dots. Adding electrons to small quantum boxes costs a certain energy and simultaneously changes the configuration of quantum states. A change in spin is also associated with a certain change in energy to minimize the energy of the many-particle ground state. For example, exchange energy is gained when electrons are added with parallel spins as compared to antiparallel spins. Depending on the characteristics of the box, a large total spin value (parallel spin filling) or a minimum total spin value (antiparallel spin filling) is

*Corresponding author.

(Fax: +81-3/5841-4162, E-mail: tarucha@phys.s.u-tokyo.ac.jp)

avored. In semiconductor quantum dots alternating spin filling [5] as well as spin-polarized filling [8] have been reported. However, it is usually difficult to assign the way of spin filling from the electronic configurations of the quantum states because of the uncertainty in the characteristic of the quantum-mechanical confinement. On the other hand, in our circular quantum dots single-particle states are well defined for a 2D harmonic potential, and using these single-particle states, we are able to assign the many-particle states from measurements of magnetic field dependence of Coulomb oscillations [5]. Furthermore, this allows us to discuss the way of spin filling for a given characteristic of the quantum states. Here, we put a special emphasis on the spin states influenced by interactions between two electrons. When the single-particle states in the dot are separated by a large energy, ΔE , an antiparallel spin filling is favored. For small ΔE , parallel spin filling is observed, which is in line with Hund's first rule. We use a magnetic field, B , to tune $\Delta E(B)$. This allows us to alter the way of spin filling. We start by using a quantum dot in a circular mesa to study the interaction effects on the spin filling. We experimentally distinguish the contributions between direct Coulomb (DC) and exchange (EX) to Hund's first rule at zero and nonzero magnetic fields and also as a function of number of electrons in the dot. We show that Hund's first rule for each shell at zero magnetic field is only associated with EX effects, whereas Hund's first rule in the presence of magnetic field is influenced by both of DC and EX effects. The obtained energies of DC and EX compare well to calculation for two-interacting electron singlet and triplet states. We then move on the rectangular mesa to discuss the effect of anisotropy in the lateral confinement on the spin states. Anisotropy in the lateral confinement gives rise to lifting of the single-particle level degeneracy present in the circular dot, and reduces the interaction effect. We measure excitation spectra of the rectangular mesa to study modifications to the spin-singlet and triplet states due to the anisotropy, and find that antiparallel spin filling is readily favored at zero magnetic field even for a small anisotropy in the lateral confinement. We calculate the energies for the level degeneracy lifting and the DC and EX interactions as a function of anisotropy in the lateral

confinement. This calculation indicates that a spin-singlet is significantly favored in an elliptic dot at zero magnetic field by the lifting of level degeneracy rather than by the reduction in the Coulomb interactions. In the presence of a magnetic field, however, we find that parallel spin filling is recovered when the single-particle level degeneracy is adjusted.

1 Quantum dot in circular mesa

1.1 Devices

We use a double-barrier structure (DBS) to fabricate vertical quantum dots [4]. The DBS consists of an undoped 12-nm $\text{In}_{0.05}\text{Ga}_{0.95}\text{As}$ well and two undoped $\text{Al}_{0.22}\text{Ga}_{0.78}\text{As}$ barriers of thickness 9.0 and 7.5 nm, and this is processed to form a circular mesa with a nominal top-contact diameter, D , of $0.54\ \mu\text{m}$. Figure 1a shows a schematic diagram of the device. Above and below the DBS there is an n -doped GaAs contact (source and drain), and the circular dot is located between the two heterostructure barriers. A single Schottky gate is placed on the side of the mesa, so it is wrapped around the dot. Figure 1b shows typical scanning electron micrographs of a circular mesa, and a rectangular mesa (discussed later) taken immediately after the deposition of the gate metal. The dot is strongly confined in the vertical direction by the heterostructures, whereas it is softly confined in the lateral direction by the Schottky-gate-induced depletion region. This depletion region is well approximated by a harmonic potential, and the characteristic energy, $\hbar\omega_0$, is evaluated from measurements of the magnetic field dependence of the Coulomb oscillations [5]. The values of $\hbar\omega_0$ obtained for various numbers of electrons in the dot are shown in Fig. 1c (The derivation of $\hbar\omega_0$ is described in Sect. 1.2). This figure clearly shows that the effective lateral confinement becomes weak as the number of electrons in the dot increases, due to the effect of Coulomb screening.

The current, I , flowing vertically through the dot is measured as a function of gate voltage, V_g , in response to a dc voltage, V , applied between the contacts. For an arbitrarily small

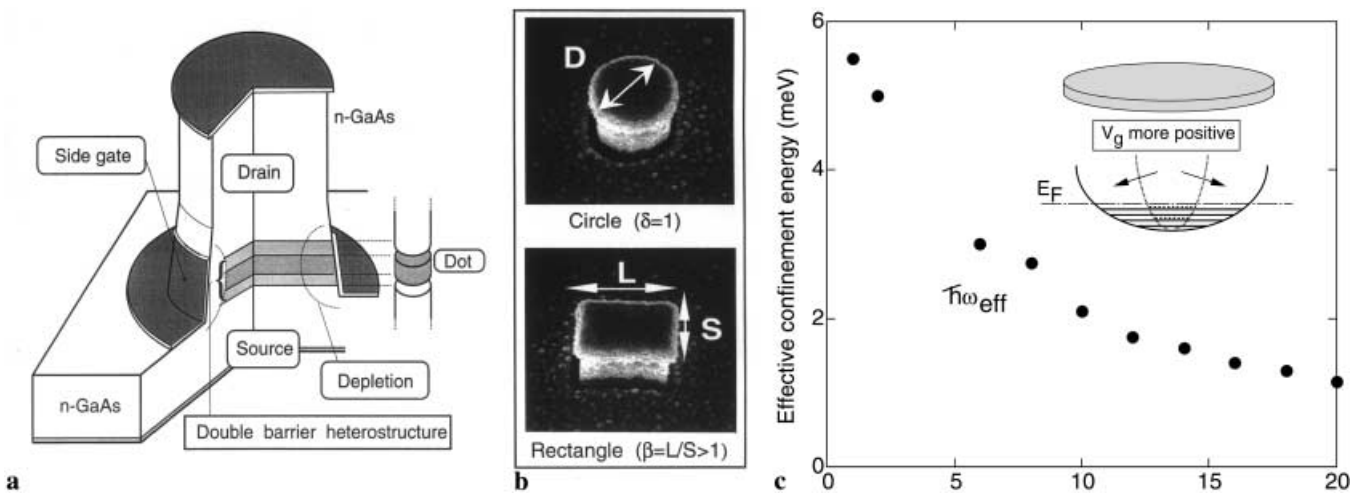


Fig. 1. **a** Schematic diagram of a quantum dot in a vertical device. The quantum dot is located inside the $0.5\text{-}\mu\text{m}$ -diameter pillar and is made from a double-barrier structure [2]. **b** Scanning electron micrographs showing submicron-sized circular and rectangular mesas. **c** Effective characteristic energy of lateral confinement, $\hbar\omega_0$, evaluated for various numbers of electrons in the circular dot. The derivation of $\hbar\omega_0$ is explained in the text

V , a series of current peaks (i.e. Coulomb oscillations) results from changing the number of electrons in the dot, N , one by one [5]. The position of a current peak for the transition from $N - 1$ to N measures the ground state (GS) electrochemical potential, $\mu(N)$. When no current flows (Coulomb blockade), the number of electrons in the dot, N , is well defined. To characterize the width of the Coulomb blockade or the spacing between peaks we define $\Delta(N) = \mu(N + 1) - \mu(N)$. The GSs and excited states (ESs) are both measured when V is set to a value sufficiently greater than the excitation energy [9]. For these measurements the sample is cooled down to about 100 mK.

1.2 N -electron ground states in the presence of magnetic field

In real atoms, electrons are so strongly trapped that their quantum mechanical properties cannot be strongly modified under normal experimental conditions, for example, by applying a magnetic field. In contrast, the electrons in our quantum dots are bound in a relatively large region of the order of 100 nm. This allows us to use readily accessible magnetic fields, not only to identify the quantum mechanical states, but also to induce transitions in the GSs whose counterparts in real atoms can never be tested on earth.

The eigenstates for a 2D harmonic quantum dot in the presence of magnetic field parallel to the current are the Fock–Darwin (FD) states [10], and are expressed by:

$$E_{n,\ell} = -\frac{\ell}{2}\hbar\omega_c + \left(n + \frac{1}{2} + \frac{1}{2}|\ell|\right)\hbar\sqrt{4\omega_0^2 + \omega_c^2}, \quad (1)$$

where n and ℓ are the radial quantum number and angular momentum quantum number, respectively, and $\hbar\omega_c = eB/m^*$ is the cyclotron energy. Figure 2a shows $E_{n,\ell}$ versus B calculated for $\hbar\omega_0 = 2$ meV. Spin splitting is neglected so

each state is two-fold degenerate. The orbital degeneracy at $B = 0$ T is lifted on initially increasing B , reflecting the first term of (1). As B is increased further, new crossings or new degeneracies can occur. The last crossing occurs along the bold line in Fig. 2a. Beyond this crossing the down-going FD-states merge to form the lowest Landau level.

Figure 2b shows the B -field dependence of the position of the current oscillations measured for the circular mesa discussed in [5]. We take into account the interaction energy as well as the FD diagram to explain the experimental data. First of all, we see a large gap (i.e. large $\Delta(N)$) between peaks for $N = 2, 6$, and 12 (also for $N = 20$ but not shown here) at $B = 0$ T. These are all signatures of complete filling of the first, second, third, and fourth shells, respectively (marked by ovals along the gate-voltage axis). The respective shells are made from degenerate $E_{n,\ell}$ states: so including spin degeneracy the first, second, third, and fourth shells respectively are twofold degenerate with $E_{0,0}$ (1s orbital), fourfold degenerate with $E_{0,1} = E_{0,-1}$ (2p orbital), sixfold degenerate with $E_{0,2} = E_{0,-2}$ (3d orbital) = $E_{1,0}$ (3s orbital), and eightfold degenerate with $E_{0,3} = E_{0,-3}$ (4f orbital) = $E_{1,1} = E_{1,-1}$ (4p orbital). We also see a relatively large gap for $N = 4$ and 9 (also for $N = 16$ but not shown here). These numbers correspond to the half filling of the second, third, and fourth shells, respectively and are consistent with Hund’s first rule.

It is also clear to see in Fig. 2b that the current peaks generally shift in pairs with B . This pairing is due to the lifting of spin degeneracy. So from the shift of the paired peaks on increasing B , we assign quantum numbers to the respective pairs. For example, the lowest, second lowest, and third lowest pairs in the vicinity of $B = 0$ T correspond to the filling of electrons in the FD states $(n, \ell) = (0, 0)$, $(0, 1)$, and $(0, -1)$ with antiparallel spins, respectively. Furthermore, the wiggles or anti-crossings between pairs of peaks correspond to the crossings of the FD states. For example, the anti-crossing

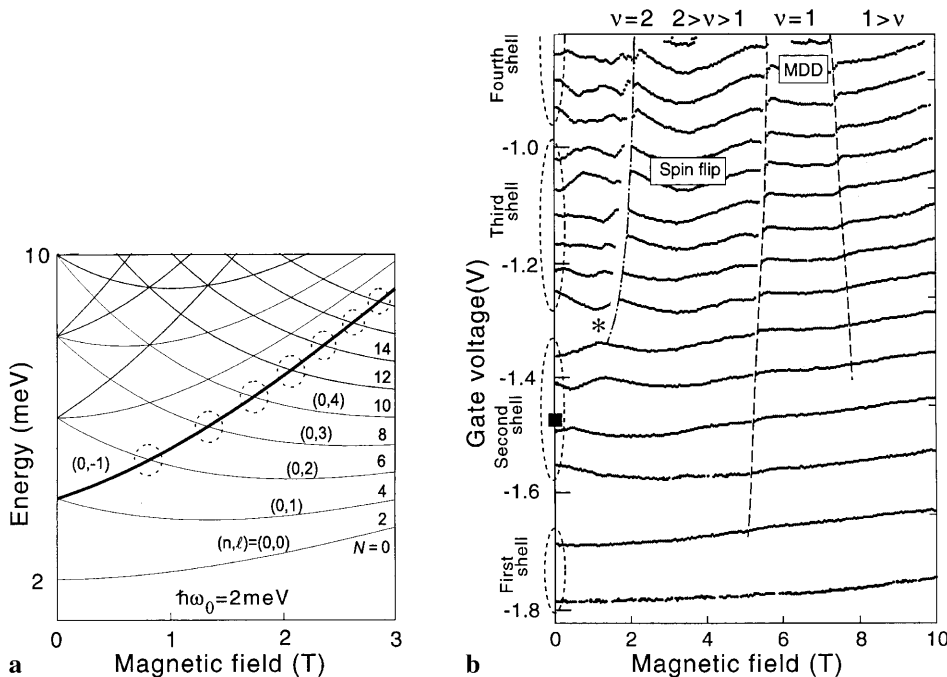


Fig. 2. **a** Fock–Darwin states calculated for $\hbar\omega_0 = 2$ meV. Dashed circles indicate the last crossing of the Fock–Darwin states. **b** B -field dependencies of current peak positions from $N = 0$ to 15. Ovals along the $B = 0$ T axis indicate groups of peaks associated with the filling of the first to the fourth shells, respectively

at the * label corresponds to the crossing of the FD states $(0, -1)$ and $(0, 2)$. However, from close inspection of the peak pairing, we find that the pairing is modified here too in line with Hund's first rule. This is discussed in detail in Sect. 2.2. The last wiggle of each pair of peaks appears along the dot-dashed line, which corresponds to the bold line in Fig. 2a. This line also identifies the filling factor $\nu = 2$. We note that the $\nu = 2$ line is more vertical in the experiment than in the calculation. This indicates that the lateral confinement becomes weaker as N increases. We calculate the FD diagram with $\hbar\omega_0$ as a fitting parameter to reproduce the $\nu = 2$ line in the experimental data. Thus we obtained $\hbar\omega_0$ for even- $N \geq 6$ and this is shown in Fig. 1c. $\hbar\omega_0$ for $N = 1$ is evaluated from the B -field dependence of the lowest peak following the $(n, \ell) = (0, 0)$ FD state, and that for $N = 2$ is evaluated from a B -field where a singlet-triplet transition (described in the following paragraph) is observed for the second lowest peak [9]. The $\hbar\omega_0$ value decreases as N increases, due to the effect of self-screening and screening of the gate metal and leads [5].

For $\nu < 2$, we see various other transitions associated with B -field-enhanced Coulomb interactions such as spin-flip transitions between $\nu = 2$ and 1 [11], a spin singlet-triplet transition when $N = 2$ at $\nu = 1$ [9, 12], and the formation of the so-called maximum density droplet (MDD) for $N \geq 2$ at $\nu = 1$ [13]. For $2 > \nu > 1$, a sequence of $N/2$ spin-flips is expected to lead to a sequential increase in the total spin of the N -electron GS from 0 to $N/2$, i.e. resulting in full spin polarization of the N -electron dot at $\nu = 1$. A self-consistent charge distribution in the dot results in a compressible center (second lowest Landau level partially filled) being separated from a compressible edge (first lowest Landau level partially filled) by an incompressible 'ring' in which the lowest Landau level is completely filled. Sequential depopulation occurs as electrons transfer across the ring from spin-down sites at the center to spin-up sites at the edge. At $\nu = 1$ MDD is formed. This is spatially the most compact state of the spin-polarized electron droplet. All N -electrons are in the lowest Landau level, and occupy sequentially the up-spin states $(n, \ell) = (0, 0), (0, 1), \dots, (0, N-1)$ without a vacancy. The detailed experiments on the spin-flip phase, and the MDD phase in our circular dot are described in [11] and [13], respectively.

2 Effects of Coulomb interactions on spin states: circular dot

2.1 Model for two interacting electrons

We first discuss a simple model that describes filling of two single-particle states with two interacting electrons. Figure 3a shows two, spin-degenerate single-particle states with energies E_a and E_b crossing each other at $B = B_0$. The GS energy, $U(1)$, for one electron occupying these states, equals E_a for $B < B_0$ and E_b for $B > B_0$ (thick line in Fig. 3a). For two electrons we can distinguish four possible configurations with either total spin $S = 0$ (spin-singlet) or $S = 1$ (spin-triplet). (We neglect the Zeeman energy difference between $S_z = -1, 0$, and 1.) The corresponding energies, $U_i(2, S)$ for $i = 1$ to 4, are given by:

$$U_1(2, 0) = 2E_a + C_{aa}, \quad (2a)$$

$$U_2(2, 0) = 2E_b + C_{bb}, \quad (2b)$$

$$U_3(2, 1) = E_a + E_b + C_{ab} - |K_{ab}|, \quad (2c)$$

$$U_4(2, 0) = E_a + E_b + C_{ab} + |K_{ab}|. \quad (2d)$$

Here, C_{ij} ($i, j = a, b$) is the DC energy between two electrons occupying states with energies E_i and E_j , and K_{ab} is the EX energy ($K_{ab} < 0$) between two electrons occupying E_a and E_b . The electrochemical potential is defined for a two-electron GS as $\mu(2) = U(2, S) - U(1)$. For each $U_i(2, S)$ we obtain potentials: $\mu_i(2) = U_i(2, S) - E_a$ for $B < B_0$ and $U_i(2) - E_b$ for $B > B_0$ (see Fig. 3b). The GS has $S = 0$ away from B_0 . Near B_0 , the lowest energy is $\mu_3(2)$, so $S = 1$. The downward cusp in the thick line identifies this spin-triplet region. The transition in the GS from $S = 0$ to 1 and $S = 1$ to 0, respectively, occurs when $\mu_1 = \mu_3$ for $B < B_0$ (labeled "S-T") and when $\mu_2 = \mu_3$ for $B > B_0$ (labeled "T-S"). We define two energies, Δ_1 and Δ_2 , to characterize the size of the downward cusp in the GS at $B = B_0$:

$$\Delta_1 = \mu_1 - \mu_3 = C_{aa} - C_{ab} + |K_{ab}|, \quad (3a)$$

$$\Delta_2 = \mu_2 - \mu_3 = C_{bb} - C_{ab} + |K_{ab}|, \quad (3b)$$

$$\Delta_1 - \Delta_2 = C_{aa} - C_{bb}. \quad (3c)$$

If the states with E_a and E_b have the same type of orbitals, EX interactions only contribute to the downward cusp since

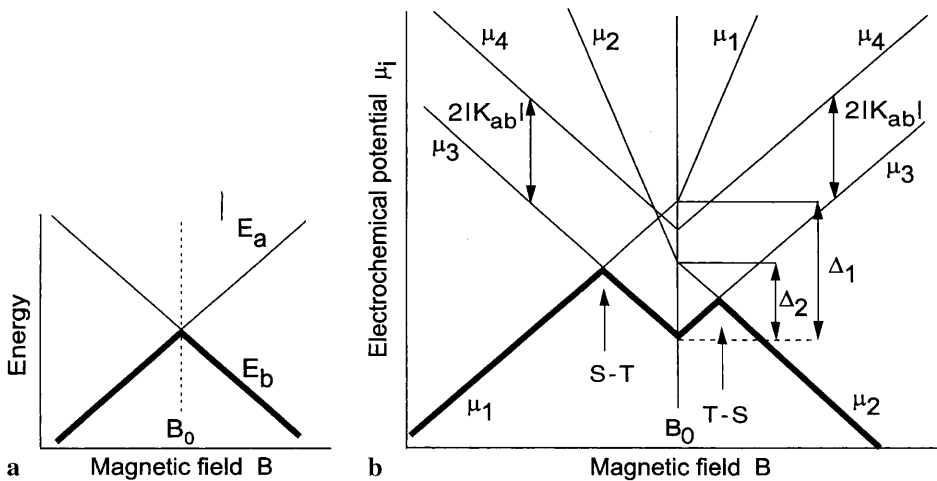


Fig. 3. **a** Schematic diagram of two single-particle states with energies E_a and E_b crossing each other at a magnetic field $B = B_0$. **b** Electrochemical potential, $\mu_i(2) = U_i(2) - U(1)$, for two interacting electrons. The *thick line* represents the ground state energy whereas the *thin lines* show the excited states

$C_{aa} = C_{bb} = C_{ab}$. This is typically the case for Hund's first rule in the second shell at $B = 0$ T, which is observed in the circular dot [5]. However, FD states at the crossings at finite fields usually have different types of orbitals, and thus $C_{aa} \neq C_{bb} \neq C_{ab}$, so both EX and DC interactions can significantly contribute to the downward cusp.

2.2 Spin singlet–triplet–singlet transition in the presence of magnetic field: experimental

In Fig. 2b we see the wiggles of paired peaks corresponding to the crossings of FD states in the low B -field range. This means that these crossings of two single-particle states, as shown in Fig. 3a, can be obtained by tuning the B -field. To examine in detail the experimental data in the vicinity of such a crossing point we show in Fig. 4a a magnified plot for the current peaks between $N = 6$ and 16 for $B = 0$ to 3 T. We see clearly the paired peaks indicating the antiparallel spin filling of a single orbital state by two electrons. Modifications to the pairing are observed for the peaks labeled by ■ at 0 T, and in each of the dashed ovals connecting pairs of peaks at non-zero field. These are all signatures of Hund's first rule; i.e. spin-polarized filling.

To demonstrate the resemblance between the data and the model of Fig. 3b, we show expansions of the evolution of the $N = 8$ and $N = 24$ peaks in Fig. 4b. The downward cusps are clearly seen. The dashed lines form a parallelogram, from which we obtain parameters Δ_1 and Δ_2 .

To compare the two-electron model with larger electron numbers, we assume that other states are far away in energy so that they can be neglected. Then, the downward cusps should occur for all higher even-electron numbers, whereas

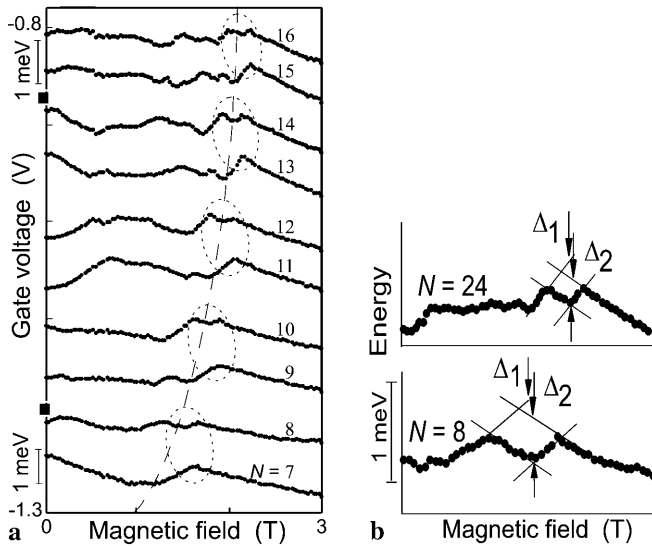


Fig. 4. **a** Magnified plot of the B -field dependencies of current peak positions from $N = 7$ to 16 shown in Fig. 2b. The bars along the gate voltage axis show 1-meV energy scales calibrated at -1.26 and -0.85 V. The long dashed curve indicates the last crossing between single-particle states. Dashed ovals group pairs of ground states for odd and even electron numbers. Spin transitions in the ground states are indicated by ■ at $B = 0$ T and occur inside the ovals for $B \neq 0$ T. **b** Magnified plots of the $N = 8$ and 24 current peaks vs. magnetic field. The dashed lines illustrate how the interaction-energy parameters, Δ_1 and Δ_2 are determined

they should be absent for all higher odd-electron numbers. This is clearly observed from the ovals in Fig. 4a. For instance, the B -field dependence of the 9th peak compares well to the thick line in Fig. 3a, i.e. a transition between two single-particle states occupied by one electron. The B -field dependence of the 10th peak compares well to the thick line in Fig. 3b, i.e. an extra downward cusp where the GS has two electrons with parallel spins ($S = 1$), occupying two different orbital states which are nearly degenerate. Other pairs of even and odd numbered peaks show the same behavior. This justifies our assumption that the other electron states can be neglected and that we can simplify the many-electron system to just one or two electrons. We note that this type of modification to peak pairing has been observed before without being identified [5, 12].

More detailed agreement of our interacting electron model with the experiment is obtained for the data of excitation spectrum. Figure 5 shows a dI/dV_g plot, taken for $V = 2$ mV. This larger voltage opens a sufficiently wide transport window between the Fermi levels of the source and drain, that both the GS and first few ESs can be detected. The GS and ESs for $N = 7$ to 9 can be assigned from the magnetic field dependence of the red or dark-red lines. Solid blue lines highlight the GSs whereas the ESs are indicated by dashed blue lines. The set of GS and ES lines for $N = 7$ shows a single crossing similar to that in Fig. 3a. The spectrum for $N = 8$ compares well to Fig. 3b and we can clearly distinguish the parallelogram formed by the GS and first ES. The downward cusp in the GS for $N = 8$ (labeled ▲) is at a slightly higher B -field than the upward cusp in the first ES (labeled ▼). This asymmetry implies that $\Delta_1 > \Delta_2$, i.e. $C_{aa} > C_{bb}$ in (3c). The same type of asymmetry is always observed along the dashed line in Fig. 4a, implying that $C_{aa} > C_{bb}$ for all N . Note that the GS for $N = 9$ appears as an upward cusp (labeled ▽) identical in form to the first ES in the spectrum for $N = 8$. This indicates that the electrochemical potential for the $N = 9$ GS is closely linked to the electronic configuration of the first ES for $N = 8$. A similar but more detailed argument is reported previously [8].

As illustrated in Fig. 4b, we can derive the experimental values for Δ_1 and Δ_2 for different N . These values are plotted as solid symbols in Fig. 6. We find that Δ_1 is larger than Δ_2 for all electron numbers, again implying that $C_{aa} > C_{bb}$. As N increases from 6 to 12, Δ_1 first increases and then slowly decreases, whilst Δ_2 slightly decreases.

The above discussion has been kept general for crossings between any type of single-particle states. To calculate DC and EX energies we use FD states calculated for the effective lateral confinement energy $\hbar\omega_0$, which changes as a function of N (see Fig. 1c)¹. As can be seen from Fig. 2a the last crossing is always a crossing between just two FD-states. The up-going state is always $(n, \ell) = (0, -1)$, whereas the down-

¹ C_{ij} and K_{ij} are the usual wavefunction overlap integrals for an unscreened Coulomb potential:

$$C_{ij} = \iint |\Psi_i(\mathbf{r}_1)|^2 \frac{e^2}{4\pi\epsilon_0 |\mathbf{r}_1 - \mathbf{r}_2|} |\Psi_j(\mathbf{r}_2)|^2 d\mathbf{r}_1 d\mathbf{r}_2,$$

$$K_{ij} = - \iint \Psi_i^*(\mathbf{r}_1) \Psi_j(\mathbf{r}_1) \frac{e^2}{4\pi\epsilon_0 |\mathbf{r}_1 - \mathbf{r}_2|} \Psi_j^*(\mathbf{r}_2) \Psi_i(\mathbf{r}_2) d\mathbf{r}_1 d\mathbf{r}_2$$

E_i and E_j are eigenvalues for the eigenfunctions Ψ_i and Ψ_j , respectively, and \mathbf{r}_1 and \mathbf{r}_2 represent the positions of the two electrons.

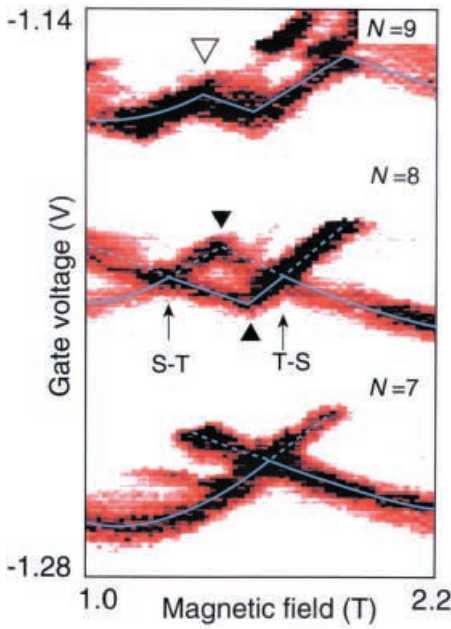


Fig. 5. dI/dV_g in the plane of V_g and B for $N=7$ to 9 measured for $V=2$ mV. $dI/dV_g > 0$ for red or dark red and $dI/dV_g \leq 0$ for white. The *solid blue lines* indicate the evolution of the GSs with magnetic field whereas the *dashed blue lines* show the ESs. The *two arrows* indicate singlet-triplet (S-T) and triplet-singlet (T-S) transitions in the GS for $N=8$

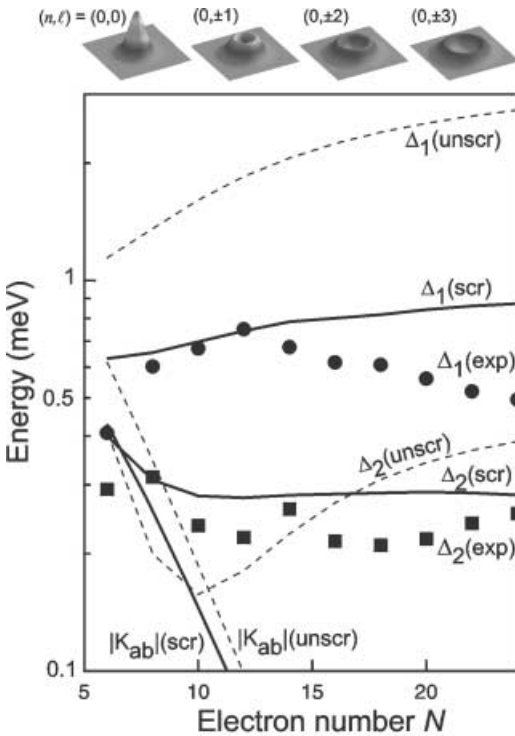


Fig. 6. Experimental values for the energy parameters Δ_1 (●) and Δ_2 (■), on a log scale, versus electron number derived from data as shown in Fig. 2a. The uncertainty in the determination of the experimental values is $\pm 10\%$ or less. The *dashed* and *solid curves* are calculated from the FD-wavefunctions at 2 T, for an unscreened (unscr) and screened (scr) Coulomb interaction. The calculated exchange energy $|K_{ab}|$ between states with energies $E_a = E_{0,-1}$ and $E_b = E_{0,N/2-1}$ decreases quickly with N . Above the *main figure* the absolute squares of the wavefunctions are shown for the relevant quantum numbers $n=0$ and $\ell=0, \pm 1, \pm 2, \pm 3$. As the angular momentum quantum number ℓ increases, the average radius increases

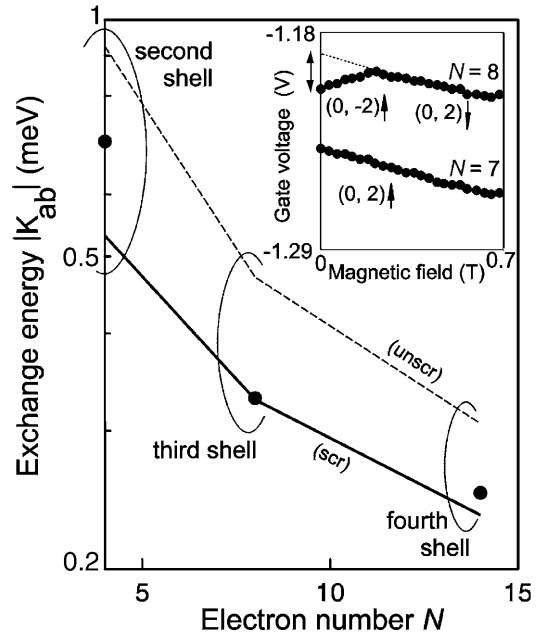


Fig. 7. Exchange energy $|K_{ab}|$, on a log scale, associated with spin-triplets formed when each new shell is filled by just two electrons at $B=0$ T. The *solid circles* are the experimental values whose uncertainty in their determination is $\pm 10\%$ or less. The *inset* shows an expansion for the filling of the first two electrons into the third shell (i.e. $N=7$ and 8). The *vertical double-arrow* represents $|K_{ab}|$ in units of gate voltage which is then converted to energy. The *calculated curves* in the *main figure* are for the unscreened (*dashed*) and screened (*solid*) cases

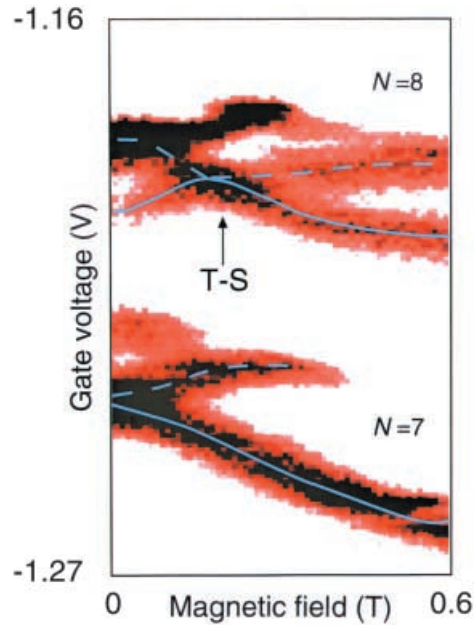


Fig. 8. dI/dV_g in the plane of V_g and B for $N=7$ and 8 in the vicinity of $B=0$ T measured for $V=1.2$ mV. $dI/dV_g > 0$ for red or dark red and $dI/dV_g \leq 0$ for white. The *solid blue lines* indicate the evolution of the GSs with magnetic field whereas the *dashed blue lines* show the ESs. The *arrow* indicates a triplet-singlet transition in the GS for $N=8$

going state, $(0, \ell > 1)$, has an increasing angular momentum for states with higher energy. (The relation with Fig. 5a is: $E_a = E_{0,-1}$ and $E_b = E_{0,\ell > 1}$.) Note that the last crossings also correspond to the thick line in Fig. 2a.

From the electron distributions of the FD-states we calculate the DC and EX energies for two electrons occupying two degenerate states. We take $\hbar\omega_0 = 2$ meV to reproduce the data for $N > 8$ and obtain Δ_1 and Δ_2 with (3a)–(3c). The dashed curves in Fig. 6 show Δ_1 and Δ_2 when we neglect screening of the interactions within the dot by electrons in the leads and in the gate. In this case the Coulomb potential falls off as $1/r$, where r is the distance between the electrons¹. For the solid curves we have approximated the screening effects by replacing the Coulomb potential by $\exp\{-r/d\}/r$. We have taken $d = 10$ nm which is roughly the thickness of the tunnel barriers. Figure 6 shows that screening considerably reduces Δ_1 to values much closer to the experimental values. Screening also removes the minimum in Δ_2 , which is also in better agreement with the experiment. For all N , we find that $\Delta_1 > \Delta_2$ and thus $C_{aa} > C_{bb}$. Since the average radius of the wavefunctions increases with angular momentum, two electrons are closer together when they both occupy $(0, -1)$ compared to when they both occupy $(0, \ell = N/2 - 1)$ for even- $N > 4$ (or $\ell > 1$), so the DC interaction is stronger in the former than the latter. This explains our observation that $C_{aa} > C_{bb}$ for all N . The overlap between different wavefunctions, $(0, -1)$ and $(0, \ell = N/2 - 1)$, decreases for even- $N > 4$ (or $\ell > 1$). This results in a decrease in both C_{ab} and $|K_{ab}|$ with N . It then follows from (3a) that Δ_1 increases until it saturates at a value equal to C_{aa} . The gradual decrease of experimental Δ_1 for $N > 12$ is probably related to the decrease in the lateral confinement with N [5] and thus the decrease in C_{aa} .

2.3 Spin singlet–triplet transition near $B = 0$ T

We now discuss the interaction effects for the $N = 4, 8$, and 14 peaks near $B = 0$ T: the $N = 4$ peak labeled ■ in Fig. 2b and the $N = 8$ and 14 peaks labeled ■ in Fig. 4a. These peaks correspond to the GS electro-chemical potentials for adding the second electron to the second, third, and fourth shells, respectively. The inset to Fig. 7 demonstrates the resemblance to the model of Fig. 3b for $N = 8$ near $B = 0$ T. Comparing the data to the FD spectrum, we assign the states such that: $E_a = E_{0,-2}$ and $E_b = E_{0,2}$. Likewise, for $N = 4$ we have $E_a = E_{0,-1}$ and $E_b = E_{0,1}$ [5] and for $N = 14$ we have $E_a = E_{0,-3}$ and $E_b = E_{0,3}$ ². These assignments are confirmed from measurements of the excitation spectrum. The data, i.e. dI/dV vs. $B - V_g$, measured for $N = 7$ and 8 near $B = 0$ T are shown in Fig. 8. (The data for $N = 3$ and 4 are shown in Fig. 12a.) The color setting for the dI/dV is the same as that in Fig. 5. The solid blue lines highlight the GSs, and the ESs are indicated by the dashed blue lines. The GS and first ES for $N = 7$ are degenerate at $B = 0$ T, and move down and up, respectively, as B is initially increased. The GS and first ES lines for $N = 8$ are exchanged at $B = 0.18$ T, indicating a transition in the ground state. Note that the states here assigned to E_a and E_b correspond to wavefunctions with a complete overlap. Also, for $B = B_0 = 0$ T the two crossing states have the same orbital symmetry implying $\Delta_1 = \Delta_2 = |K_{ab}|$; i.e. only EX effects contribute to the downward cusp (Note that the asymmetry ($\Delta_1 \neq \Delta_2$) can only occur for $B_0 \neq 0$).

² For $N = 14$ it is difficult to identify the corresponding state since the B -dependence is not clear enough to distinguish between $E_{0,-3}$ and $E_{1,-1}$. We assume it is $E_{0,-3}$, and continue to evaluate $|K_{ab}|$

We derive $|K_{ab}|$ as illustrated in the inset to Fig. 7 from the intersection with the $B = 0$ T axis of the dashed line and the measured data. Figure 7 shows that the EX energy quickly becomes smaller for higher lying shells. For comparison we also show the calculated screened and unscreened values for the EX energy. The screened case provides the best quantitative agreement for our realistic choices of the confining energy and the screening distance.

Our general model used for the calculations in Figs. 6 and 7 provides a clear identification of effects due to EX and DC interactions. An important simplification is the reduction of a many-electron system to just two interacting electrons. We note that there are more advanced calculations supporting our analyses [14].

3 Effects of deformation in the lateral confinement

3.1 Deformed dots in rectangular mesa

A rectangular mesas with top contact area ($L \times S$), 0.55×0.4 μm , is prepared from the same DBS wafer. $L(S)$ is the nominal dimension of the longest (shortest) side of the top contact [6, 15]. A simple way to classify the rectangular mesa is to define a geometric parameter, β , to be the ratio L/S ($= 1.375$). Due to a slight undercut, the area of the mesa is a little less than that of the top contact. Figure 9a shows schematically the slabs of semiconductor between the two tunneling barriers, and the resulting dot bounded by the shaded depletion region.

As illustrated in Fig. 9a, the lateral confining potential of the dot inside the rectangular mesa is expected to be approximately elliptical due to rounding at the corners provided the number of electrons in the dot is not too large, or too small [6, 15]. Assuming the confining potential is still perfectly parabolic: $(1/2)m^*(\omega_x^2 x^2 + \omega_y^2 y^2)$, we choose to characterize the ‘ellipticity’ by a deformation parameter, $\delta = E_x/E_y$. Here, $E_x(E_y)$ is the confinement energy at 0 T along the major (minor) axis ($E_x = \hbar\omega_x > E_y = \hbar\omega_y$). The 2D states in the elliptical dot are labeled by the quantum numbers (n_x, n_y) , where n_x (n_y) is the principal quantum number ($= 0, 1, 2, \dots$) associated with the energy parabola along the major (minor) axis. The energy of single-particle state (n_x, n_y) is $(n_x + 1/2)E_x + (n_y + 1/2)E_y$.

For a perfectly circular mesa, we trivially generalize our definition of δ so that $\delta = \beta = 1$. On the other hand, for the rectangular mesa, there is no simple correspondence between β , a ratio of lengths characteristic of the top metal contact, and δ , a ratio of energies characteristic of the dot in the mesa, and β is dependent on V_g (or equivalently N). Nevertheless, although we are not saying that $\delta = \beta$, we assume that β is a ‘measure’ of δ .

3.2 Magnetic field dependence

Figure 9b–d shows the B -field evolution up to 6 T of the first 10 single-particle energy levels for elliptical dots ($\delta = 1.5, 2, 3.2$) calculated according to the model described by Madhav and Chakraborty [7] with a fixed confinement energy of $E_Q = 3$ meV [15]. The confinement energies for the elliptical dot are simply derived from the relation $E_x E_y = E_Q E_Q$. Quantum numbers (n_x, n_y) for some of the states are indicated.

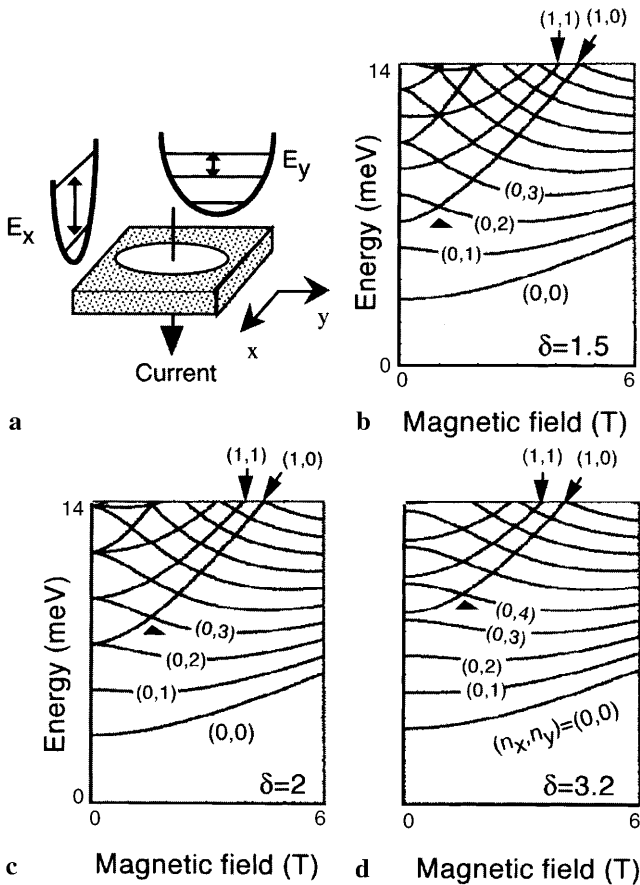


Fig. 9. a Schematic diagram of the lateral confinement potential assumed for a dot in the rectangular mesa. b–d Calculated B -field dependence of the first ten single-particle energy levels for elliptical dots with $\delta = 1.5, 2,$ and 3.2

As the deformation is gradually increased, Figs. 9b–d, degeneracies of the single-particle states at 0 T are generally lifted, although accidental degeneracies can occur at certain ‘magic’ deformations, provided the confining potential remains perfectly parabolic. A weak B -field parallel to the current can also induce degeneracies of the single-particle levels in a similar manner to that for a circular dot. As discussed before, ‘wiggles’ in the position of pairs of current peaks are expected at weak field because of these crossings. The first lowest energy ‘wiggle’ originates from the crossing marked by \blacktriangle in Figs. 9b–d, and this crossing moves to higher energy (N) and higher B -field with increasing δ . The evolution of each single-particle energy level on initial application of B -field is weaker for larger deformation. The spectra also highlight that the single-particle energy level spacing generally decreases as δ increases.

Figure 10 shows the B -field dependence of the Coulomb oscillation peak positions measured for the rectangular mesa [15]. The data consists of current vs. V_g traces taken at a very small bias at different B -fields. Peaks are paired, and there are no obvious deviations close to 0 T for $N = 4$ due to Hund’s rule. Quantum numbers (n_x, n_y) of the single-particle states are assigned, and the first up-moving pair of peaks is marked by the solid arrow. In the single-particle picture, the first up-moving state is $(n_x, n_y) = (1, 0)$.

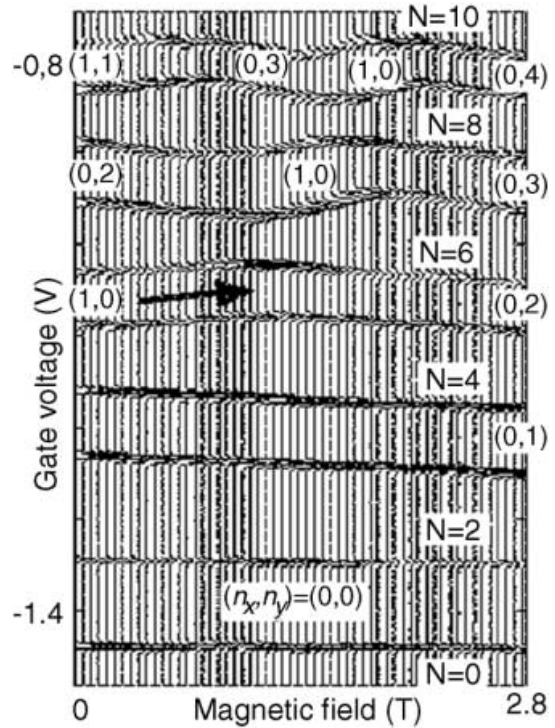


Fig. 10. B -field dependences of the current peak positions measured for $N = 0$ to 10 for the rectangular mesa. The bias voltage V is sufficiently small that only the ground states are detected

We also prepared rectangular mesas with larger β , and from the same measurements as shown in Fig. 10, we find that there is a reasonable correspondence between the measured position of the first up-moving pair of peaks and lowest energy wiggle, and trends predicted from the calculation shown in Fig. 9. This leads to an estimate of δ in the rectangular mesa we discuss here: $1 < \delta < 2$. Detailed discussion on the relation between the values of β and δ , in different rectangular mesas are described in [15].

3.3 Influence on spin states

In Fig. 10 we see no clear modification to the peak pairing for $N = 0$ to 10 near $B = 0$ T. In particular this indicates that the spin-state for $N = 4$ is a singlet. This spin-singlet is also confirmed from measurements of the Zeeman shift [6]. For a circular dot at $N = 4$ the $(n, \ell) = (0, 1)$ and $(0, -1)$ states are degenerate at 0 T and their wavefunctions have the same symmetry, but with deformation this degeneracy is lifted and these states become the $(n_x, n_y) = (1, 0)$ and $(0, 1)$ states in an elliptical dot (which are split at 0 T). This energy splitting, γ , increases with δ . At the same time, the effect of DC and EX interactions are both reduced since overlap of the wavefunctions becomes smaller. Note that γ depends more strongly on the deformation than the interaction energies (see Fig. 12b). For a small deformation, if $\gamma < E_{EX}$ (E_{EX} is the energy gain due to EX in the circular dot) at 0 T, EX can still operate to lower the energy, and thus the $N = 4$ GS remains a spin-triplet. On the other hand, if $\gamma > E_{EX}$ at 0 T, the GS is a spin-singlet, so normal pairing is expected [7, 15]. Thus, we can expect a triplet–singlet transition at some critical deformation. The absence of deviations to the normal peak pairing

at $N = 4$ in Fig. 10 apparently confirms that δ is greater than $1.2 - 1.3$ in line with previous calculations [7, 15].

Detailed information on the effect of deformation in the rectangular mesa can be obtained from measurements of the excitation spectra. Figure 11 shows the excitation spectrum for the circular mesa (a) and for the rectangular mesa (b). GSs and ESs for $N = 3$ and 4 are indicated in dI/dV_g vs. $B - V_g$ plotted in the same way as for Fig. 8. For the circular mesa, the GS and first ES lines for $N = 3$ follow the B -field dependence of FD states $(n_x, n_y) = (0, 1)$ and $(0, -1)$, respectively, and the spectrum for $N = 4$ is consistent with a crossing of the FD states $(0, 1)$ and $(0, -1)$ at 0.4 T. This crossing identifies the singlet-triplet transition in the GS. In contrast, there is no signature of the single-triplet transition for $N = 4$ in the spectrum of the rectangular mesa. In addition, for both

$N = 3$ and 4, the GS and first ES are widely spaced at 0 T, and follow the B -field dependence of states $(n_x, n_y) = (0, 1)$ (down-moving state) and $(1, 0)$ (up-moving state), respectively (see Fig. 9b). The splitting between the GS and first ES is 0.8 meV for $N = 4$ at 0 T. This energy is smaller by 0.8 meV than the same splitting for $N = 3$, mainly due to the contribution of EX energy.

To investigate the effect of deformation on the GS and ES observed in Fig. 11 we calculate the contributions of the lifting of level degeneracy and change in Coulomb interactions using the same assumptions as employed for the calculations in Figs. 6 and 7. Figure 12a shows the calculated total energy needed for adding an extra electron to the $N = 2$ GS as a function of deformation δ . Here we use $\hbar\omega_0$ of 3 meV to reproduce the confining energy when $N = 3$ (see Fig. 1c). This total en-

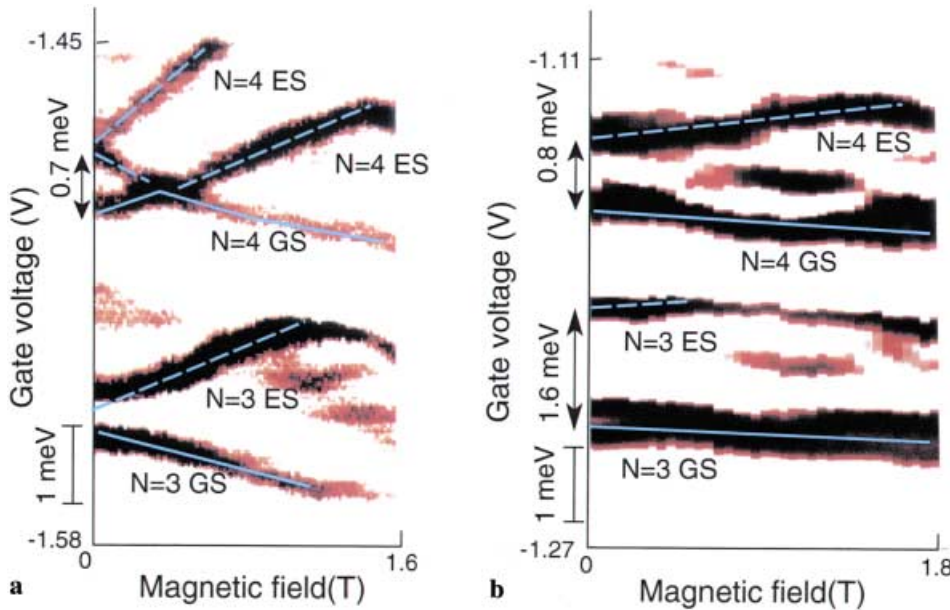


Fig. 11a,b. dI/dV_g in the plane of V_g and B for $N = 3$ and 4 measured for the circular mesa (a) and the rectangular mesa (b). V is set at 1.6 mV. $dI/dV_g > 0$ for red or dark red and $dI/dV_g \leq 0$ for white. The solid blue lines indicate the evolution of the GSs with magnetic field whereas the dashed blue lines show the ES

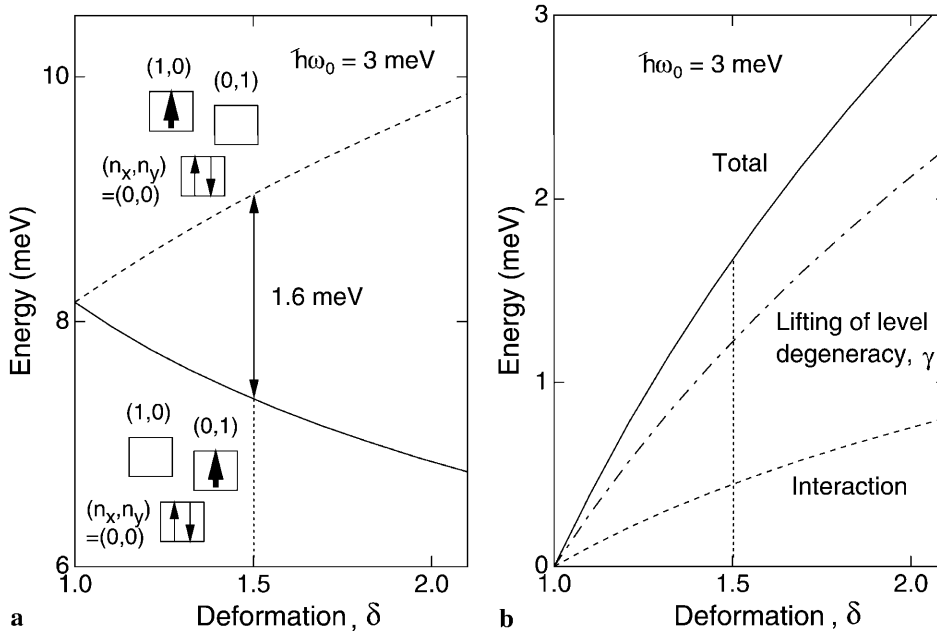


Fig. 12. a Calculation of energies needed for adding an extra electron into two different configurations from the two-electron ground state of an elliptic quantum dot. The lower- and higher-lying lines are the ground and first excited states, respectively, and the corresponding configurations are pictorially illustrated. The bold arrow indicates the “added electron”. **b** Contributions from lifting the level degeneracy (dot-dashed line) and changes in interaction energies (dashed line) to the energy difference (solid line) between the two different configurations shown in a

ergy incorporates the energy, γ , lifting of level degeneracy and the energy of interaction between the added third electron, and the residing two electrons for $N = 2$ GS, which is made from an orbital state $(n_x, n_y) = (0, 0)$ occupied by two antiparallel spin electrons. Note that in our previous calculation of the electrochemical potential $\mu_i(2)$ for two-electrons in the circular dot (see Fig. 3b) we neglected the influence of the existing electrons on the different two-electron configurations ($i = 1$ to 4) since there is no big difference in the spatial form of these two-electron configurations. However, this assumption becomes invalid when the dot contains a large deformation in the lateral confinement. The GS, and first ES for $N = 3$ are formed by adding an extra electron to a state $(n_x, n_y) = (0, 1)$ and $(1, 0)$, respectively. The wavefunction for state $(n_x, n_y) = (1, 0)$ (or $(0, 1)$) is extended along the x (or y) direction as compared to that for state $(n_x, n_y) = (0, 0)$. However, the degree of the extension is significantly smaller for state $(n_x, n_y) = (1, 0)$. So the interaction effect between the third electron and the residing two electrons in the $N = 2$ GS is stronger for the state $(n_x, n_y) = (1, 0)$ than that for the state $(n_x, n_y) = (0, 1)$. In Fig. 12a the calculated energies are degenerate for the GS and ES at $\delta = 0$ and becomes more widely spaced as the deformation increases. This energy spacing is a measure of the energy difference between the GS and first ES, obtained in the experiment of excitation spectrum, and thus from comparison with the experimental data for $N = 3$ at 0 T we can estimate a deformation of $\delta = 1.5$ for our rectangular mesa. In Fig. 12b contributions to the splitting of the GS and ES shown in Fig. 12a are distinguished for the level degeneracy lifting, γ , and the interaction energy. As the deformation increases, the interaction energy decreases for the GS, while it increases for the ES. The increase in γ with deformation is significantly stronger than that of the interaction energy. So we conclude that the GS for $N = 3$ in

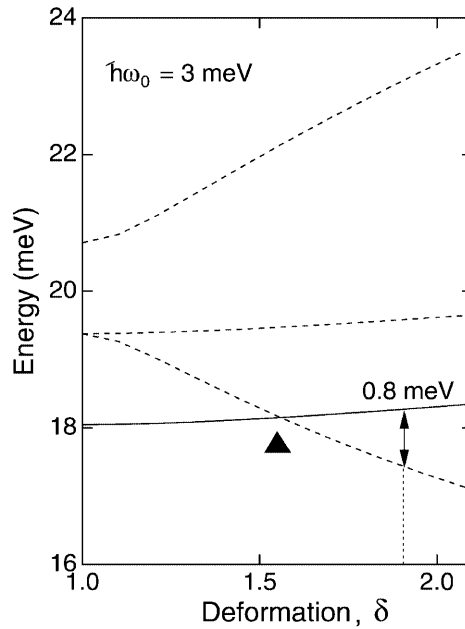


Fig. 13. Calculation of energies needed for adding two extra electrons into the different configurations from the two-electron ground state of a quantum dot with anisotropy in the lateral confinement. The *solid line* is a spin-triplet, whereas the *dashed lines* are all spin-singlets. The *lowest-lying line* is always the ground state and the *higher lying lines* are all the excited states

our rectangular mesa is mainly influenced by the lifting of the level degeneracy between states $(n_x, n_y) = (0, 1)$, and $(1, 0)$ and only partially by the reduction in the interaction effect.

For the $N = 4$ GS and ES we also show the calculation of the energy needed for putting two extra electrons into the GS for $N = 2$ in Fig. 13. Here we consider four possible

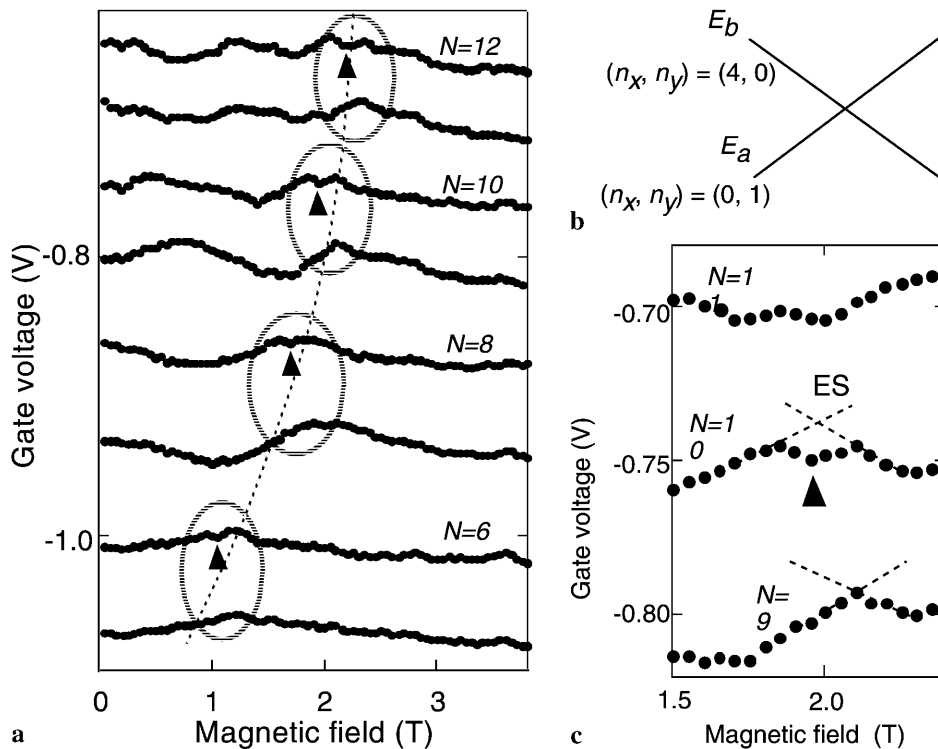


Fig. 14. **a** B -field dependencies of current peak positions measured for $N = 5$ to 12 for the rectangular mesa. The bias voltage V is sufficiently small to detect only the ground states. The *dotted line* indicates the last crossing between single-particle states. *Dotted ovals* group pairs of ground states for odd and even electron numbers. Spin singlet-triplet-singlet transitions in the ground states occur at the \blacktriangle labels in the ovals for $B \neq 0$ T. **b** Schematic of two-single particle states $(n_x, n_y) = (1, 0)$ with $(0, 4)$ crossing each other, which accounts for the B -field dependence of the ground state for $N = 9$ in **c**. **c** Magnified plots of the $N = 9$ to 11 current peaks vs. magnetic field. A downward cusp, a signature of spin transition, is marked by \blacktriangle . The *dashed lines* illustrate the excited states (spin singlet) in the region of the downward cusp

configurations for a small deformation: one configuration for the spin-triplet and three configurations for the spin-singlet. The triplet state has two parallel spins in two different orbital states $(n_x, n_y) = (0, 1)$ and $(1, 0)$. On the other hand, the singlet state has two antiparallel spins either in two different orbital states $(n_x, n_y) = (0, 1)$ and $(1, 0)$ or in the same orbital state of $(n_x, n_y) = (0, 1)$ (or $(n_x, n_y) = (1, 0)$). In this figure the GS is the triplet for a small deformation, but a transition from triplet to singlet occurs at $\delta = 1.55$. From a comparison to the excitation spectrum for $N = 4$ we estimate $\delta = 1.9$. The values obtained from the calculation shown in Fig. 12, (a) for $N = 3$ and (b) for $N = 4$ are both consistent with $1 < \delta < 2$ evaluated from the B -field dependence of the current peak positions in Fig. 10. This δ value for $N = 4$ is somewhat larger than that evaluated from the excitation spectrum for $N = 3$. This discrepancy may reflect a functional dependence of δ on N , but is more likely to be due to an inaccuracy in the calculation since this calculation becomes less valid as δ becomes greater than 1.5.

Our calculation for the GSs and ESs in the elliptic dot is very simple, however, it is still useful for understanding the experimental data. There are more refined calculations reported elsewhere. Numerical diagonalization has been successfully employed to calculate basic electronic properties of dots with anisotropic confining potentials [7]. Such ‘exact’ calculations, however, are limited to $N \leq 6$. For a larger number of electrons, spin-density functional theory is a powerful technique, which explicitly incorporates the electron–spin interactions [7, 15]. Both approaches predict changes in the addition energy spectra, and transitions in the spin-states as the deformation is varied.

In rectangular mesas, even for a small deformation a spin-singlet is favored by the lifting of level degeneracy at $B = 0$ T. We can still tune the single-particle levels with a magnetic field to highlight interaction effects related to the spin-triplet in the same way as discussed for the circular mesa. Figure 14a shows the evolution of current peaks with magnetic field for $N = 5$ to 12. Modifications to the usual pairing of neighboring peaks, i.e., anti-ferromagnetic filling, are observed inside each of the dashed ovals connecting pairs of peaks at non-zero field. These ovals are located along the last crossing of the single-particle state $(n_x, n_y) = (1, 0)$ with $(0, n_y)$ ($n_y \geq 2$). The upper peak inside the dashed oval shows a small but definite downward cusp which is a signature of the singlet–triplet–singlet transition. For example, a downward cusp is clearly seen for $N = 10$ at 2 T in the magnified plot in Fig. 14c. The size of the downward cusp is smaller in the rectangular mesa than that for the circular mesa, probably due to the reduction in both of DC and EX interactions in the rectangular mesa.

4 Conclusions

We have used vertically gated circular and rectangular mesas to study the effects of Coulomb interactions on the spin states in quantum dots. The circular mesa contains a circular quantum dot with a high degree of rotational symmetry and parabolicity in the lateral confinement. This gives rise to systematic sets of degenerate single-particle levels at zero magnetic field. The filling of these degenerate states leads to atom-like properties such as shell filling and the obedience of

Hund’s first rule. Application of a magnetic field parallel to current leads to systematic modifications in the energy spectrum, and these modifications are well reproduced in terms of the Fock–Darwin spectra. By adjusting the level degeneracy as a function of magnetic field, we observe parallel spin filling as favored by the direct Coulomb and exchange interactions at non-zero magnetic field. This means that electrons tend to have parallel spins in line with Hund’s first rule when they occupy nearly degenerate single-particle states. The influence of the direct Coulomb and exchange interactions on the spin-configurations are well explained in terms of two-electron singlet and triplet states. On the other hand, for the rectangular mesa, the quantum dot is subject to elliptical anisotropy in the lateral confinement. This lifts the level degeneracy and reduces the interaction energy, both of which favor antiparallel spin filling. Consequently, there are no signatures of parallel spin filling observed for the rectangular mesa at zero magnetic field. This is attributed mainly to the lifting of the level degeneracy rather than the weaker reduction in the interaction energy. On the other hand, parallel spin filling can still be induced when the level degeneracy is adjusted as a function of weak magnetic field.

Acknowledgements. We thank T. Honda, R. van der Hage, J. Janssen, T. Oosterkamp, H. Tamura, and T. Uesugi for their help and useful discussions. We would also thank S.M. Reimann, M. Koskinen and M. Manninen for their discussions on the effect of anisotropy in the lateral confinement of a quantum dot. S.T. and L.P.K. acknowledge financial support from Grant-in-Aid for Specially Promoted Scientific Research and also for Scientific Research on the Priority Area of “Single Electron Devices and Their High Density Integration” from the Ministry of Education, Science, Sports and Culture in Japan, from CREST-FEMD(JST), from the Dutch Organization for Fundamental Research on Matter (FOM), and from the NEDO program NTDP-98.

References

1. S. Tarucha, Y. Hirayama, T. Saku, Y. Tokura: Proc. of the Int. Workshop on Science and Technology of Mesoscopic Structures, ed. by S. Namba, C. Hamaguchi, T. Ando (Springer, Hong Kong 1992) p. 243
2. For reviews, *Mesoscopic Phenomena in Solids*, ed. by B.L. Altshuler, P.A. Lee, R.A. Webb (Elsevier, 1991); U. Meirav, E.B. Foxman, *Semicond. Sci. Technol.* **11**, 255 (1996); Proc. of the NATO Advance Study Institute on Mesoscopic Electron Transport, ed. by L.L. Sohn, L.P. Kouwenhoven, G. Schoen (Kluwer, Dordrecht, Netherlands, Series E, **345**, 105, 1997)
3. M. Reed: *Scientific American* **268**, 118 (1993); M.A. Kastner: *Phys. Today* **46**, 24 (1993); R.C. Ashoori: *Nature* **379**, 413 (1996)
4. D.G. Austing, T. Honda, S. Tarucha: *Semicond. Sci. Technol.* **11**, 1995 (1995)
5. S. Tarucha, D.G. Austing, T. Honda, R.J. van der Hage, L.P. Kouwenhoven: *Phys. Rev. Lett.* **77**, 3613 (1996); S. Tarucha, T. Honda, D.G. Austing, Y. Tokura, K. Muraki, T.H. Oosterkamp, J.W. Janssen, L.P. Kouwenhoven: *Physica E* **3**, 112 (1998)
6. See experiments in: S. Tarucha, D.G. Austing, T. Honda, R.J. van der Hage, L.P. Kouwenhoven: *Jpn. J. Appl. Phys.* **36**, 3917 (1997); S. Sasaki, D.G. Austing, S. Tarucha: *Physica B* **256–258**, 157 (1998)
7. See calculations on single-particle states in: A.V. Madhav, T. Chakraborty: *Phys. Rev. B* **49**, 8163 (1994); interaction effects using exact diagonalization approach in: T. Ezaki, Y. Sugimoto, N. Mori, C. Hamaguchi: *Semicond. Sci. Technol.* **13**, A1 (1998); using spin density functional theory in: S.M. Reimann, M. Koskinen, M. Manninen: *Phys. Rev. B* **59**, 1613 (1999); S.M. Reimann, M. Koskinen, J. Kolehmainen, M. Manninen, D.G. Austing, S. Tarucha: *Eur. J. Phys. D* **9**, 105 (1999)
8. D.R. Stewart, D. Sprinzak, C.M. Marcus, C.I. Duruoec, J.S. Harris Jr.: *Science* **278**, 1784 (1997)

9. L.P. Kouwenhoven, T.H. Oosterkamp, M.W.S. Danoesastro, M. Eto, D.G. Austing, T. Honda, S. Tarucha: *Science* **278**, 1788 (1997)
10. V. Fock: *Z. Phys.* **47**, 446 (1928); C.G. Darwin: *Proc. Cambridge Philos. Soc.* **27**, 86 (1930)
11. P.L. McEuen, E.B. Foxman, J. Kinaret, U. Meirav, M.A. Kastner, N.S. Wingreen, S.J. Wind: *Phys. Rev. B* **45**, 11 419 (1992); P.L. McEuen, N.S. Wingreen, E.B. Foxman, J. Kinaret, U. Meirav, M.A. Kastner, Y. Meier, S.J. Wind: *Physica B* **189**, 70 (1993); P. Hawrylak, C. Gould, A. Sachrajda, Y. Feng, Z. Wasilewski: *Phys. Rev. B* **59**, 2801 (1999); see for our disk-shaped dot in: D.G. Austing, Y. Tokura, T. Honda, S. Tarucha, M. Danoesastro, J. Janssen, T.H. Oosterkamp, L.P. Kouwenhoven: *Jpn. J. Appl. Phys.* **38**, 372 (1999)
12. First proposal is given by: M. Wagner, U. Merkt, A.V. Chaplik: *Phys. Rev. B* **45**, 1951 (1992); see for experimental evidence in: B. Su, V.J. Goldman, J.E. Cunningham: *Phys. Rev. B* **46**, 7644 (1992); R.C. Ashoori, H.L. Stoermer, J.S. Weiner, L.N. Pfeiffer, K.W. Baldwin, K.W. West: *Phys. Rev. Lett.* **71**, 613 (1993)
13. A.L. MacDonald, S.R.E. Yang, M.D. Johnson: *Aust. J. Phys.* **46**, 345 (1993); see for our circular dot in: T.H. Oosterkamp, J.W. Janssen, L.P. Kouwenhoven, D.G. Austing, T. Honda, S. Tarucha: *Phys. Rev. Lett.* **82**, 2931 (1999)
14. There are various calculations consistent with our experiment; exact calculation for $N < 7$ by: A. Wojs, P. Hawrylak: *Phys. Rev. B* **53**, 10 841 (1996); M. Eto: *Jpn. J. Appl. Phys.* **36**, 3924 (1997); Hartree-Fock calculations for $N > 8$ by: A. Natori, Y. Sugimoto, M. Fujito: *Jpn. J. Appl. Phys.* **36**, 3960 (1997); H. Tamura: *Physica B* **249–251**, 210 (1998); M. Rontani, F. Rossi, F. Maghi, E. Molinari: *Phys. Rev. B* **59**, 10 165 (1999); Spin density-functional theory at $B = 0$ T by: I.-H. Lee, V. Rao, R.M. Martin, J.-P. Leburton: *Phys. Rev. B* **57**, 9035 (1998); M. Koskinen, M. Manninen, S.M. Reimann: *Phys. Rev. Lett.* **79**, 1817 (1997); and also at non-zero B by: O. Steffen, U. Rossler, M. Suhrke: *Europhys. Lett.* **42**, 529 (1998)
15. D.G. Austing, S. Sasaki, S. Tarucha, S.M. Reimann, M. Koskinen, M. Manninen: *Phys. Rev. B* **60**, 11 514 (1999)